

Fog Intermittency and Critical Behavior

Kelly Y. Huang ^{1,*}, Gabriel G. Katul ², Thomas J. Hintz ¹, Jesus Ruiz-Plancarte ³, Qing Wang ³
and Harindra J. S. Fernando ¹

¹ Civil and Environmental Engineering and Earth Sciences, University of Notre Dame, Notre Dame, IN 46556, USA

² Civil and Environmental Engineering, Duke University, Durham, NC 27708, USA

³ Meteorology Department, Naval Postgraduate School, Monterey, CA 93943, USA

* Correspondence: yhuang28@nd.edu

Abstract: The intermittency of fog occurrence (the switching between fog and no-fog) is a key stochastic feature that plays a role in its duration and the amount of moisture available. Here, fog intermittency is studied by using the visibility time series collected during the month of July 2022 on Sable Island, Canada. In addition to the visibility, time series of air relative humidity and turbulent kinetic energy, putative variables akin to the formation and breakup conditions of fog, respectively, are also analyzed in the same framework to establish links between fog intermittency and the underlying atmospheric variables. Intermittency in the time series is quantified with their binary telegraph approximations to isolate clustering behavior from amplitude variations. It is shown that relative humidity and turbulent kinetic energy bound many stochastic features of visibility, including its spectral exponent, clustering exponent, and the growth of its block entropy slope. Although not diagnostic, the visibility time series displays features consistent with Pomeau–Manneville Type-III intermittency in its quiescent phase duration PDF scaling ($-3/2$), power spectrum scaling ($-1/2$), and signal amplitude PDF scaling (-2). The binary fog time series exhibits properties of self-organized criticality in the relation between its power spectrum scaling and quiescent phase duration distribution.

Keywords: dynamical model; fog; intermittency; self-organized criticality; sporadic randomness



Citation: Huang, K.Y.; Katul, G.G.; Hintz, T.J.; Ruiz-Plancarte, J.; Wang, Q.; Fernando, H.J.S. Fog

Intermittency and Critical Behavior. *Atmosphere* **2023**, *14*, 875. <https://doi.org/10.3390/atmos14050875>

Academic Editor: Thierry Bergot

Received: 23 March 2023

Revised: 27 April 2023

Accepted: 15 May 2023

Published: 17 May 2023



Copyright: © 2023 by the authors. Licensee MDPI, Basel, Switzerland. This article is an open access article distributed under the terms and conditions of the Creative Commons Attribution (CC BY) license (<https://creativecommons.org/licenses/by/4.0/>).

1. Introduction

Fog occurrence is associated with saturated water vapor and accompanying water droplets near the earth's surface, causing visibility to drop below 1 km [1]. This reduction in visibility raises numerous logistic and safety issues for aviation, seafaring, and transportation. Ecologically, fog plays an underappreciated role through its transport of water droplets, aerosols, and microorganisms, which impacts the thermodynamic, hydrologic, photosynthetic, and nutrient properties of ecosystems [2,3]. The potential for fog as a potable water source has also been proposed and explored [4,5]. Fog formation continues to receive attention in viticulture, as sustained moist conditions modulate the microclimate and promote mildew disease and fungal infection [3].

A key aspect in fog statistics is its intermittency, the switching between fog and no-fog phases (on–off switching properties), which was shown to be related to the long-term persistence of fog events with a characteristic time scale that appears invariant [6]. Intermittency in precipitation, a process that similarly exhibits on–off switching properties between rain and no-rain events, has received copious attention in literature and has been modeled using stochastic point processes [7,8], multiplicative cascades [9,10], and traditional stochastic models [11]. More recently, Rigby and Porporato [12] found that summer convective rainfall exhibits features of Pomeau–Manneville Type-III intermittency, an example of a sporadically random process (a behavior between periodicity and pure randomness). Further, rainfall has been shown as an example of self-organized criticality (SOC) [13], which

started with the original work of Bak and Chen [14]. In contrast, limited attention has been afforded to dynamic models in fog, and this limitation motivated the current work.

A recent study proposed some similarities between rainfall and fog statistics at coarse time scales [15]. Motivated by these results, the work here seeks to explore the extent to which existing dynamical models for precipitation apply to fog occurrences by comparing several scaling relations that describe the fog time series to those that have been noted in the literature. High-resolution time series of visibility Vis taken over a one-month period is used to explore the analytic relations concerning the power laws in the spectral density, the distribution of the off phases, and the distribution of the event sizes for phenomenological comparison to the proposed dynamical models. In addition, the current study also seeks to explore atmospheric variables that could possibly contribute to the intermittency of fog occurrences. To this end, time series of air relative humidity RH and turbulent kinetic energy k , which may provide conditions for the formation and break-up of fog, respectively, are also analyzed herein in the same framework to draw connections between these atmospheric variables and the proposed dynamical models. This analysis will serve as a first step to developing stochastic models for fog, which can be employed in fog simulation studies, to check physical models, and to explore underlying formation processes of fog.

1.1. Types of Dynamical Intermittency

Intermittency is a route to chaos in dynamical systems and is characterized by the irregular alternation between phases of regular, almost periodic behavior (“laminar” phases) and phases of chaotic dynamics (“turbulent” phases). As a control parameter exceeds a critical value, the system eventually becomes fully chaotic without laminar phases. Models of different types of intermittency have been classified and observed in various systems [16,17].

Pomeau and Manneville [18] described three types of intermittency (Types I–III) caused by linear instabilities of periodic trajectories, where Pomeau–Manneville Type I intermittency (PM1I) is associated with an inverse tangent bifurcation, Type II (PM2I) with a Hopf bifurcation, and Type III (PM3I) with a period-doubling bifurcation. PM1I has been observed in numerical studies of ordinary differential equations and discrete dynamical systems [19–21] and in specialized experiments [22–25]; PM2I in numerical and experimental studies of nonlinear oscillators [26,27] and in a hydrodynamical system [28]; and PM3I in biological systems [29,30], electrical applications [31–34], rainfall time series [12], and at the onset of hydrodynamic turbulence [35].

On–off intermittency is another model that describes a time series characterized by switching between near-constant “off” phases punctuated by burst phases of large deviations caused by sudden instabilities [36], and has been observed in many mathematical models [36–39], electrical circuits [40,41], spin wave instabilities [42], gas discharge plasma systems [43], and the electroconvection of nematic liquid crystals [44]. Other models not considered here include Type V [45,46], Type X [47], multi-intermittency [48] and crisis-induced intermittency [49].

For comparison of phenomenological features of these intermittency models with those of fog time series, the analytic properties related to the distribution of the duration of the quiescent or laminar phases, power spectral density, and distribution of event size (or signal amplitudes) can be explored, which are summarized in Table 1. The distribution of the duration of the laminar phases has been used in the literature to differentiate between types of intermittency. PM3I and on–off intermittencies generate probability distribution functions (PDFs) of the quiescent phases $PDF(l)$ that decay as a power law with an exponent of $-3/2$ (that is, $PDF(l) \sim l^{-3/2}$) at small l , while PM2I generates ones with an exponent of -2 at small l followed by an exponential tail (or cutoff) at larger l [50]. In contrast, PM1I is expected to show a power law decrease with an exponent of $-1/2$ for small l followed by an increase at large l [50].

Table 1. Phenomenological features of intermittency models under consideration, where PDF refers to the probability density function, l is the duration of the laminar or quiescent phases, f is the frequency or inverse time scale, x is the event size, and E_x is the spectral density function .

	PM Type-I	PM Type-II	PM Type-III	On-off
PDF(l)	$l^{-1/2}$	l^{-2}	$l^{-3/2}$	$l^{-3/2}$
$E_x(f)$	$(f \log_{10}f ^2)^{-1}$	$f^{-1/2}$	$f^{-1/2}$	$f^{-1/2}$
PDF(x)	x^{-1}	x^{-2}	x^{-2}	x^{-1}

Procaccia and Schuster [51] showed that the power spectral density $E_x(f)$ scales as $(f|\log_{10}f|^2)^{-1}$ in a PM1I process and as $f^{-1/2}$ in a PM2I or a PM3I process for $f \rightarrow 0$ by considering their 1-D local Poincaré maps [18], where f is the frequency (or inverse time scale). Venkataramani et al. [52] demonstrated that the power spectrum of an on-off intermittent process with no noise exhibits a power law decay with an exponent of $-1/2$ over an intermediate range of frequencies dependent on the system constants. Lastly, the PDF of the signal amplitude (or event size), $PDF(x)$, is considered. On-off intermittency shows a decay in $PDF(x)$ with an exponent of -1 for small x [53], PM1I with an exponent of -1 , and PM2I and PM3I with an exponent of -2 [54].

More generally, Pomeau–Manneville intermittency maps and their stochastic counterparts have been shown to be examples of sporadic randomness. Based on the entropic characteristics of trajectories, Gaspard and Wang [54] defined a class of sporadically random dynamical systems that reside between periodicity (processes that generate repeating sequences) and regular randomness (processes whose complexity grows linearly with sequence length, i.e., Markov chains and Brownian motions, which have a convergent entropy rate). Sporadic random processes display a strong memory while retaining a stochastic component, and the complexity grows as a power law with the sequence length.

1.2. Self-Organized Criticality

Generally, phase transitions occur when the control or tuning parameter (an ambient property) is varied across its critical value so that the order parameter (a macroscopic, measurable property) exhibits a jump in its values. The phase transition is of the first order if the order parameter varies discontinuously (i.e., a discontinuous change in entropy at a fixed temperature corresponding to latent heat), and of the second order if it varies continuously but not analytically (i.e., the transition is marked by a sharp corner on the phase diagram).

In second-order continuous phase transitions, the system can reside at criticality, a state between two qualitatively different types of behavior. Since phase transitions typically separate an ordered state from a less ordered one, systems at criticality are often said to be on the edge of chaos, and have been shown to exhibit optimal memory and processing capabilities (for a review, see [55]). Further, in systems where the tuning and order parameters are coupled, the critical point can become an attractor so that the system tunes itself as it evolves toward criticality, in a behavior termed self-organized criticality (SOC) [14]. In SOC, the system is driven toward a second-order phase transition, wherein the dynamics is driven by universal properties. For an SOC system at criticality, a relation is expected between the spectral exponent and the power law decay of the quiescent phases. Controversies notwithstanding, SOC has been shown to be a possible candidate for a wide variety of systems in physical, biological, and social sciences, spanning from climate fluctuations [56] and neural systems [57] to wars [58] (for a complete review, see [59–61]). Similar to the physical analogy laid out by Peters and Neelin [13] for rainfall, it can be argued that a critical value of RH (the tuning parameter) marks the continuous phase transition to a regime of fog events.

2. Methods

2.1. Measurements

Measurements were collected on Sable Island (43.9337° N, 59.9149° W), a small North Atlantic island located approximately 300 km southeast of Halifax, Nova Scotia (see Figure 1), as part of the Fog and Turbulence Interactions in the Marine Atmosphere (FATIMA) field campaign. The site was chosen for its proximity to the Grand Banks region, which is identified to have one of the climatologically highest marine fog occurrences with a peak of 45% during June–July–August [62]. The island’s maximum elevation above sea level is 30 m, making it an ideal location for collecting data without significantly disturbing the marine sea fog advecting past it. Data were collected from 1 to 31 July 2022, during which fog (horizontal visibility ≤ 1 km) was observed approximately 25% of the time.

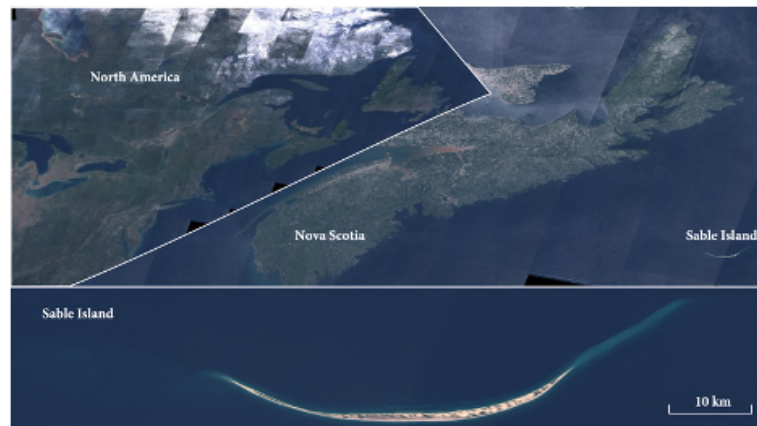


Figure 1. Location of Sable Island in the Grand Banks region of the North Atlantic Ocean (**top**). Sable Island is shown in the inset (**bottom**). Images were taken by the Sentinel-2 multispectral satellite.

Longitudinal (U), transverse (V), and vertical (W) velocities were collected with a triaxial sonic anemometer (Campbell Scientific IRGASON) at a height of 2 m above the ground. Corrections to the sonic anemometer data were applied to account for line path averaging and flow distortion by the sonic transducers [63,64]. A low-pass filter was then applied to avoid high-frequency noise, and subsequent turbulence data were processed using 5-min windows. Gaps in velocity data due to rain were filled using a moving average over a one-hour window, and then again with a one-day window. Turbulence kinetic energy k is then calculated as

$$k = \frac{1}{2} \left(\overline{(u')^2} + \overline{(v')^2} + \overline{(w')^2} \right), \quad (1)$$

where u' , v' , and w' are the longitudinal, transverse, and vertical fluctuating velocity components, respectively, and the overbar denotes averaging over a 5-min period.

Visibility (Vis) and relative humidity (RH) time series were collected at 15-s intervals using a forward scatter sensor (Vaisala FD70) and the attached humidity probe (Vaisala HMP155), respectively, located approximately 20 m west of the sonic anemometer at a measurement height of 2.5 m (see Figure 2). Here, visibility is used as a proxy for the intensity of fog, with Vis being inversely proportional to the liquid water content [65]. Visibility and relative humidity data are also down-sampled to 5-min averages.

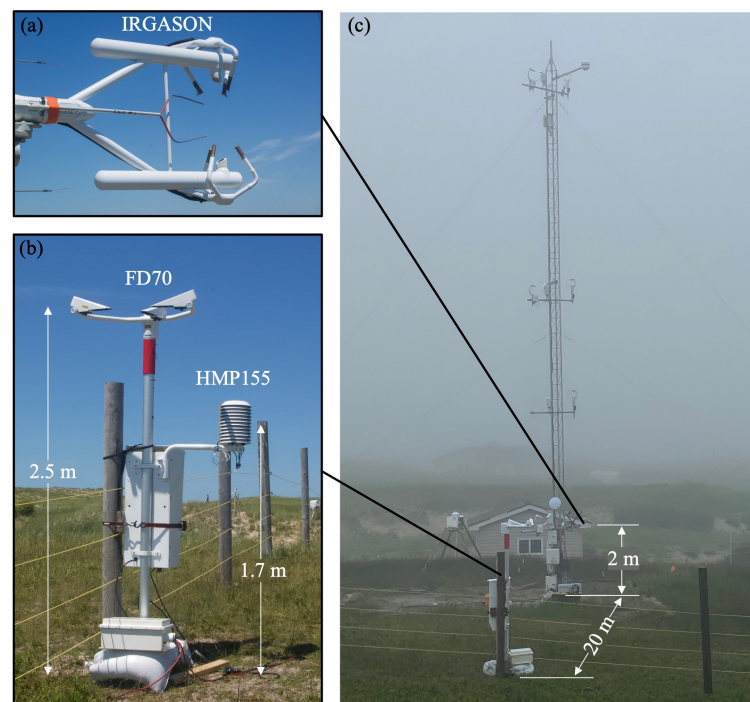


Figure 2. Photos of the IRGASON (a) and the FD70 with an attached HMP155 (b). The IRGASON is mounted on a measurement tower at a height of 2 m, and the FD70 is located 20 m west of the measurement tower with a measurement height of 2.5 m for *Vis* and 1.7 m for *RH* (c). The figure is created by the author.

2.2. Analysis Methods

To analyze intermittency statistics, the telegraph approximation (TA) is used. The TA of a time series $s(t)$ isolates its clustering behavior from its amplitude variations by transforming it into a binary series:

$$\text{TA}(s(t)) = \frac{1}{2} \left(\frac{s(t) - s^*}{|s(t) - s^*|} + 1 \right), \quad (2)$$

where $\text{TA}(s(t))$ takes on a value of 1 when $s(t)$ exceeds a threshold s^* and a value of 0 otherwise. As it retains only threshold-crossing (on–off or off–on switching) information, the TA series contains no information about magnitude variation. Here, $k^* = |k| = 0.61 \text{ m}^2/\text{s}^2$, $Vis^* = 1000 \text{ m}$ (to reflect the definition of fog occurrence so that $\text{TA}(Vis) = 1$ when $Vis \leq 1000 \text{ m}$ and $\text{TA}(Vis) = 0$ otherwise), and $RH^* = 100\%$ (to reflect saturation so that $\text{TA}(RH) = 1$ when $RH \geq 100\%$ and $\text{TA}(RH) = 0$ otherwise).

Telegraph approximation has been used in turbulence research [66,67] to quantify clustering and intermittency behavior in studies of temperature, velocity, and scalar concentration fluctuations in the atmospheric surface layer, within canopies, and across several surface roughness, density and thermal stratification [68–74]. The same method has also been applied to the study of rainfall intermittency [75]. Sreenivasan and Bershadskii [67] showed empirically from several numerically generated stochastic series that when the power spectra of the original series scales as f^{-n} and that of the TA series as f^{-m} ,

$$m = \frac{n + 1}{2}, \quad (3)$$

where f is, as before, the frequency, n is the spectral exponent of the original series, and m is the spectral exponent of the TA series. This relation appears to hold across a broad range of stochastic processes. Generally, $m < n$ (that the spectra of the TA decays slower than that of the original series) indicates that there is more ‘memory’ in the TA series such that

amplitude variations seem to have “decorrelating” effects on the series. The spectra were calculated using standard fast Fourier transforms from the normalized time series

$$s_n(t) = \frac{s(t) - \overline{s(t)}}{\sigma_s}, \tag{4}$$

where the overbar denotes the mean, and σ_s is the root mean square value of $s(t)$. The window length is set to half of the time series length.

The cluster exponent α characterizes the clustering tendency of the time series and is determined from the scaling of the local standard deviation of the density of threshold-crossings $\langle \delta n_\tau^2 \rangle^{1/2}$ with τ :

$$\langle \delta n_\tau^2 \rangle^{1/2} \sim \tau^{-\alpha}, \tag{5}$$

where $\delta n_\tau = n_\tau - \langle n_\tau \rangle$, n_τ is the average density of zero-crossings within a time interval τ (i.e., the number of threshold crossings normalized by the number of points in that time interval), and angled brackets denote time averaging for window size τ . While a white noise process (that has no clustering tendencies in its zero crossings) has a cluster exponent of $\alpha = 0.5$, Sreenivasan and Bershadskii [67] showed that $\alpha \rightarrow 0.1$ (finite clustering persists) as the Taylor microscale Reynolds number $Re_\lambda \rightarrow \infty$ in turbulent flows.

The intermittency exponent μ can be calculated from the local average of the variance dissipation rate of a signal $s(t)$ in a time interval τ ,

$$\xi_\tau = \frac{1}{\tau} \int_t^{t+\tau} \left| \frac{ds(t)}{dt} \right|^2 dt, \tag{6}$$

as

$$\frac{\langle \xi_\tau^q \rangle}{\langle \xi_\tau \rangle^q} \sim \tau^{-\mu_q}. \tag{7}$$

A uniform random distribution of pulses yields $\mu_q = 0$, while an intermittent series yields non-zero μ_q values. Here, only μ_2 ($q = 2$) is considered, and the subscript is dropped henceforth. Calculated from the full series, μ_s contains information on both clusterization and amplitude variations, while μ_{TA} calculated from the TA series retains only clusterization information. Thus, their relative magnitudes indicate the role of amplitude variations and clusterization in the observed intermittency. That is, $\mu_{TA} < \mu_s$ indicates that amplitude variations amplify the intermittency; $\mu_{TA} > \mu_s$ indicates that amplitude variations mitigate intermittency; and for $\mu_{TA} \approx \mu_s$, much of the observed intermittency is due to the on-off and off-on properties but not amplitude variability.

The rate of growth of the complexity of a trajectory in time classifies a process as periodic, random, or sporadically random. A conventional method to quantify this growth of complexity for discrete time series is to study the information content of the systems (information theory). Consider a sequence A with symbols a_i , where $i = 0, \dots, \lambda$, from a given alphabet. The sequence A is considered periodic if some symbols or sub-sequences occur repeatedly, and disordered (or random) when all of its symbols occur with equal frequency. This can be measured by the Shannon entropy [76]:

$$H = - \sum_i p_i \log p_i, \tag{8}$$

where p_i is the probability that symbol a_i occurs at any position. To reflect the correlations between the symbols, Equation (8) can be generalized to obtain the block entropy

$$H(n) = - \sum_i p_i^{(n)} \log p_i^{(n)}, \tag{9}$$

where $p_i^{(n)}$ are the probabilities of the combinations of n symbols. For periodic processes with period τ , the block entropy reaches a constant and stops growing (entropy rate becomes zero) at $n > \tau$. For purely random processes, the entropy grows linearly with n ,

reflecting the constant level of uncertainty with each additional step. Thus, for a sporadic random process, where the system is always yielding information and decreasing the uncertainty in the next step but never reaching complete regularity, the entropy grows sub-linearly without reaching a plateau. Therefore, a relation $H(n) \propto n^\beta$, with $0 \leq \beta \leq 1$ is expected [54]. Here, to maximize the value of n available without significant finite-size effects, the binary TA signal is used to limit the alphabet to binary (0 and 1) and, subsequently, the number of possible sequences to 2^n . The maximum n is then determined as $n_{max} = \log_2[N/100]$ so that the estimate would be sensitive to sequences of probability on the order of 0.01.

The connection to SOC in the current study arises because the PDF of the duration of the quasi-regular or “laminar” phases, and the PDF of the event sizes both exhibit power law scaling, i.e., $PDF(l) \sim l^{-\gamma}$ and $PDF(x) \sim x^{-\beta}$. In particular, for SOC systems near critical behavior, Jensen et al. [77] showed that

$$m = 3 - \gamma \quad (10)$$

using the classical sandpile model near critical slopes. To account for intermittency effects, Bershadskii et al. [66] modified this relation to

$$m = 3 - \gamma - \mu/2, \quad (11)$$

where μ is the intermittency correction calculated using squared temporal gradients as in Equation (7).

3. Results

3.1. Overview

Figure 3 presents the time series of RH , k , Vis , and their corresponding TA series over the experimental period. Relative humidity values greater than 100% were observed and could be attributed to the reported sensor inaccuracy of $\pm 1.7\%$ RH . Nonetheless, the study at hand concerns only the switching across saturation, and RH^* values of $100 \pm 1.7\%$ do not significantly alter the conclusions presented below. It can be seen that fog occurrence ($Vis \leq 1000$ m) generally follows high RH and low k . To explore the combined effect of these two criteria, an additional “ $RH^1 k_0$ ” TA series was calculated by assigning a value of 1 only when both $TA(RH) = 1$ and $TA(k) = 0$. Analysis of this series will be discussed below.

Binned scatter-plots of Vis against RH and k are presented in Figure 4 with the colormap indicating the density of points. Bin sizes are 0.5% for RH , $0.03 \text{ m}^2/\text{s}^2$ for k , and 400 m for Vis . A linear fit between Vis and RH yielded a coefficient of determination $R^2 = 0.63$. In contrast, Vis and k appear uncorrelated ($R^2 = 0.0045$). Nonetheless, the highest density of points for $Vis \leq 1000$ m occurs for low k , indicating that low turbulence levels are well correlated with fog occurrences.

3.2. Spectra

The spectra of both the original and the TA series of RH , k , and Vis are presented in Figure 5. The spectrum for RH shows a peak at 24 h, which could arise from diurnal variation. As a result, the frequency range corresponding to 22–26 h was excluded when calculating the power laws for RH . A mild bump at 24 h can also be seen in the spectrum for Vis , which could be a signature of night-time fog that disappears in the morning.

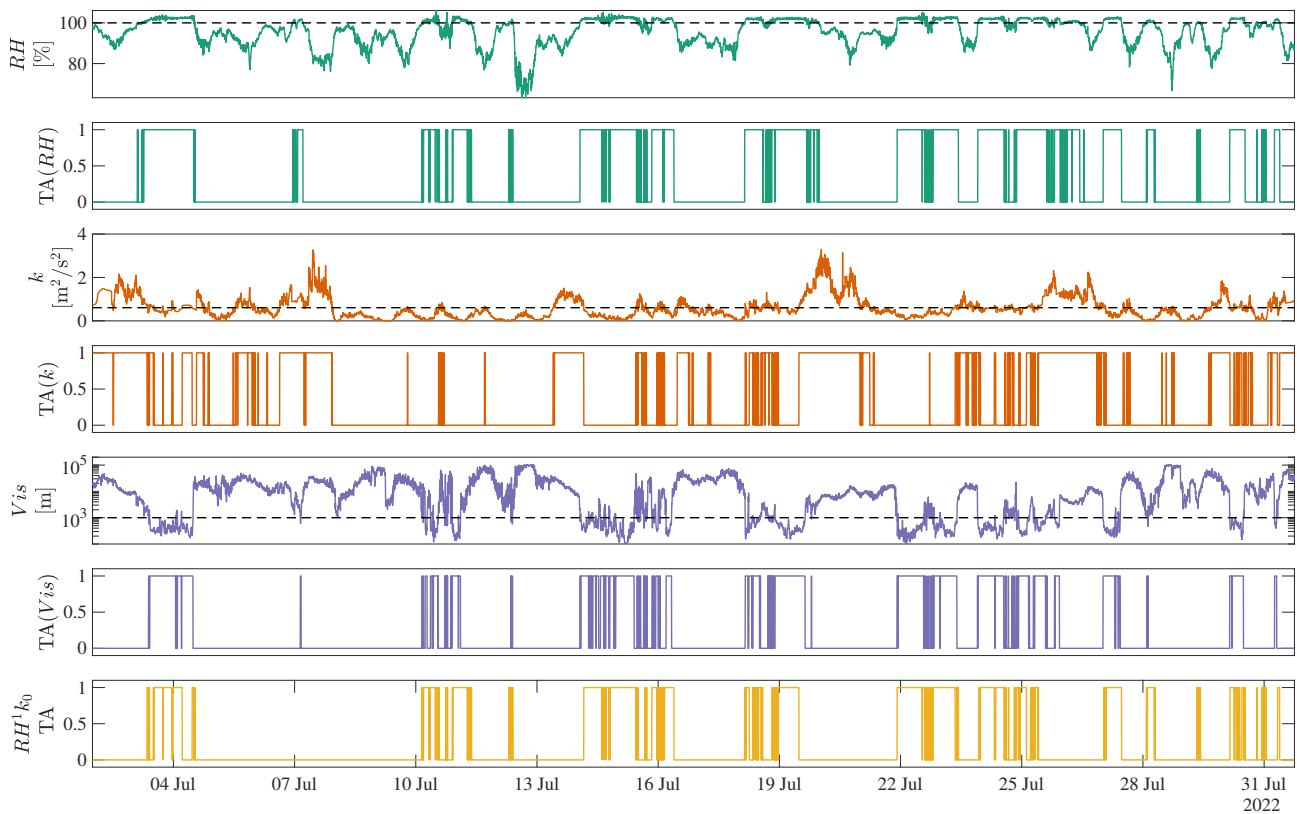


Figure 3. Time series of RH , k , and Vis and their corresponding TA series over the sampling period. Dashed lines in the original series indicate the thresholds ($RH^* = 100$, $k^* = |k| = 0.61 \text{ m}^2/\text{s}^2$, and $Vis^* = 1000 \text{ m}$) used in Equation (2). The last row presents the combined RH^1k^0 TA series.

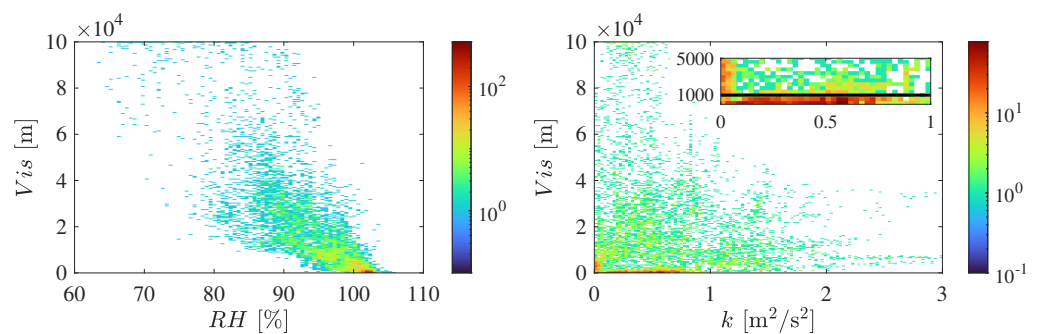


Figure 4. Binned scatter-plots of Vis against RH (left) and against k (right) with the colormap indicating the density of points.

All spectra appear to exhibit three regimes of power-law scaling, separated at 24 h and at 1 h. Of the three regimes, the fastest decay appears to occur within the frequency range of 1–24 h, while the spectra for time scales >24 h and <1 h decay at a slower rate. Hereafter, we label the frequencies associated with time scales >24 h as slow, <1 h as fine, and bounded between daily and hourly as intermediate. Returning to spectral exponents, the spectral slope n approaches a value of $-1/2$ for the slow regime in Vis but not in RH or k . Generally, for the slow scales, the Vis series exhibits a shallower slope in its spectra than RH or Vis . The spectrum of the combined RH^1k^0 TA series exhibits similar slopes to k in its intermediate and fine scales and to RH in its slow scales.

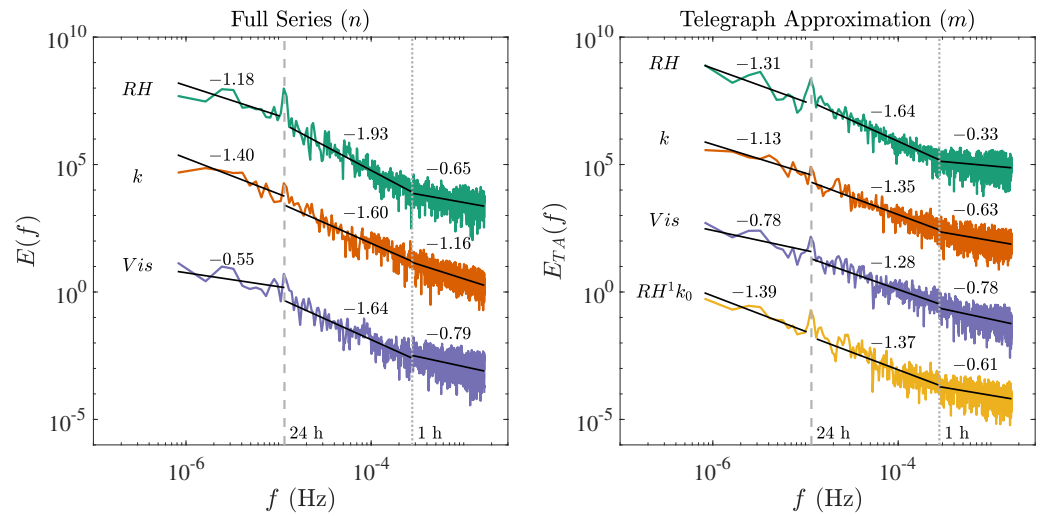


Figure 5. Energy spectra of the full (left) and TA (right) series of all three variables. The spectra have been offset to permit comparisons. Time scales of 24 h (---) and 1 h (---) delineate the scaling regimes.

Overall, the relation between spectral exponents m and n reasonably follow Equation (3) (see Figure 6). For the slow time scales, $m > n$ was observed in both RH and Vis , meaning that there is less “memory” in the TA series and that amplitude variations have correlating effects. For the intermediate and fine time scales (<24 h) in RH and Vis , and for all time scales in k , the spectra of the TA series decay slower than that of its corresponding full series ($m < n$), meaning that amplitude variations seem to have de-correlating effects at those time scales. Thus, much of the power law scaling may be due to the memory in the switching between on-off and off-on instead of the amplitude variations.

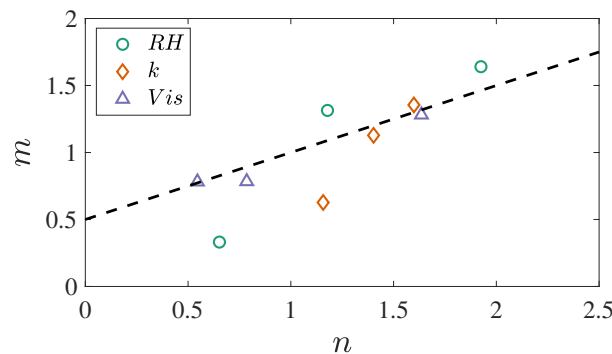


Figure 6. A plot of the spectral exponents of the original series (n) and of the corresponding TA series (m) for all three variables and all three scaling regimes indicated in Figure 5. The dashed line indicates the relation in Equation (3).

As a preliminary indicator of the extent to which variability in RH and k is correlated with Vis , the magnitude-squared coherences C of the full and TA series are presented in Figure 7. In addition, the additive effect of RH and k in explaining Vis is considered in $C_{Vis, RH^1 k_0}$ calculated between Vis and a mixed model based on the linear combination of RH and k (with each normalized to span from 0 to 1). Similarly, $C_{TA(Vis), TA(RH^1 k_0)}$ considers the coherence between $TA(Vis)$ and the combined $RH^1 k_0$ TA series. The coherences are smoothed through bin averaging to highlight the underlying trends.

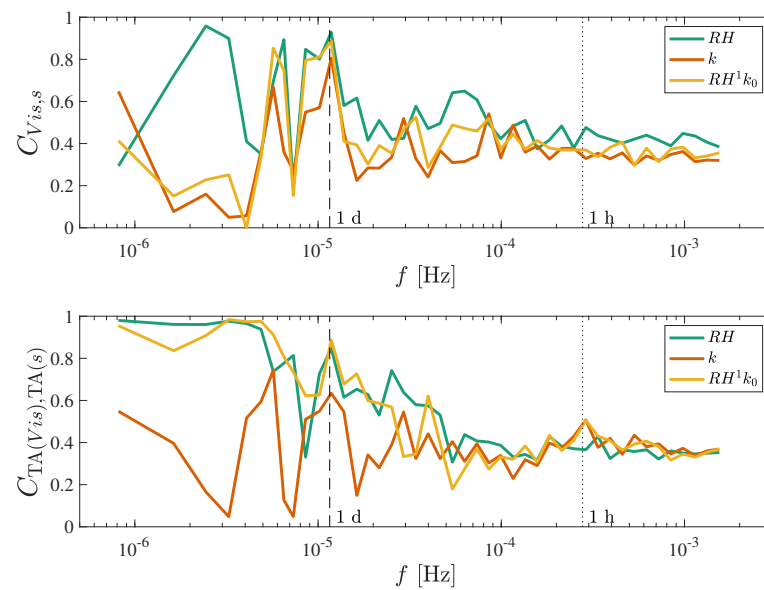


Figure 7. Squared coherence $C_{Vis,s}$ between Vis and the two control variables $s = RH$ and $s = k$ (and their combination) as a function of frequency f (**top**). The analysis is repeated for the TA series (**bottom**). The squared coherence measures how correlated Vis is to a control variable at a given f . Note the similarity in $C_{Vis,s}$ for the original and TA series at intermediate and fast time scales.

For the slow time scales of the full series, $C_{Vis,RH}$ exhibits peaks (>0.8) at the 5 d, 2 d, and 1 d time scales (showing that the spectra of fog can be reasonably predicted from the spectra of relative humidity at these time scales), while $C_{Vis,k}$ exhibits a minimum (<0.2) so that the spectra of fog are not related to those of k in this region. For the slow time scales of the TA series, it appears that the behavior of Vis is captured by that of RH ($C_{TA(Vis),TA(RH)}$ approaches 1 for time scales >2 d). The combined $RH^1 k_0$ TA series appears to only marginally improve the correlation to Vis near the 1 d time scale. For fine and intermediate time scales, both RH and k (and their combined effect) exhibit $C \approx 0.4$ in both the full and TA series, indicating that although RH and k behaviors are somewhat correlated to that of Vis , neither is able to fully explain the variability in Vis . These results further prompt the current analysis into its intermittency structure and the possible models beyond the activation and inhibition mechanisms of fog.

3.3. Cluster Exponents

Standard deviations of the zero-crossing density fluctuations δn_τ as a function of τ are featured in Figure 8. All TA series exhibit clear power law scaling with a break in scaling behavior, resulting in two regimes. Generally, there is significant clustering ($\alpha = 0.24 - 0.26$) for larger time scales followed by almost no clustering ($\alpha = 0.5$ consistent with a white noise process). The break between these two regimes occurs at $\tau \approx 12$ h for RH , k and $RH^1 k_0$, and at $\tau \approx 24$ h for Vis . Surprisingly, the cluster exponent for Vis ($\alpha = 0.25$) is consistent with those reported in [15], where $\alpha = 0.26$ and $\alpha = 0.25$ based on deposition data from a fog collector at a coastal and an inland site, respectively, for $\tau < 5$ days.

The intermittency exponents μ_s and μ_{TA} are presented in Figure 9. All TA series show similar levels of intermittency ($\mu_{TA} = 0.42 - 0.44$). For RH and Vis , $\mu_{TA} > \mu_s$ shows that amplitude variations mitigate intermittency and have 'correlating' effects. In contrast, $\mu_{TA} \approx \mu_s$ for k shows that much of the intermittency in k originates from its on-off and off-on switching properties.

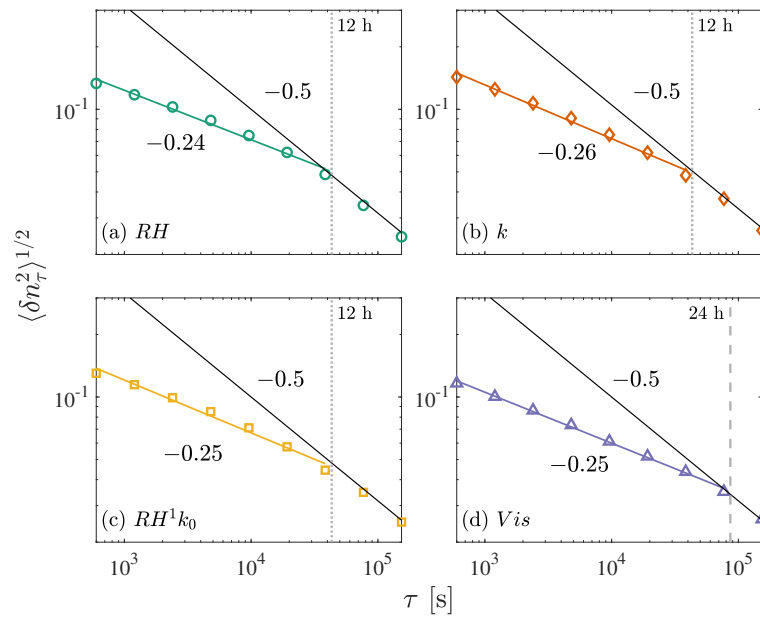


Figure 8. Standard deviations for the running threshold-crossing density fluctuations for *RH* (a), *k* (b), *Vis* (c), and $RH^1 k_0$ (d) series as function of window size τ . Best-fits that indicate the power laws and the scaling for a white noise process ($\alpha = 0.5$) are indicated with straight black lines. The separation of the two scaling regions is also indicated for each variable with a vertical dashed line.

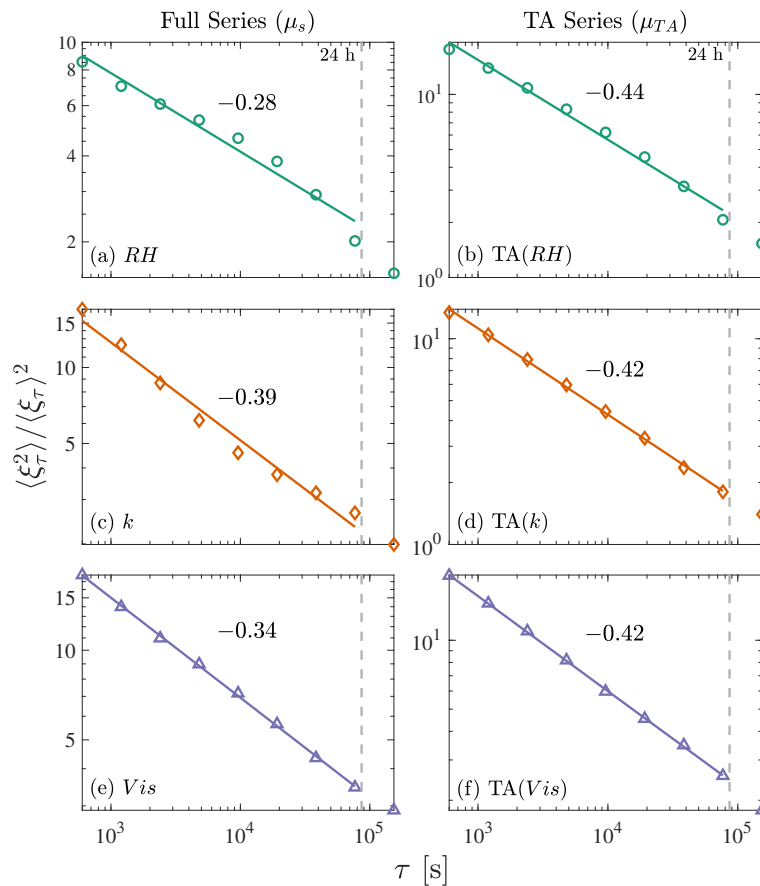


Figure 9. Normalized second moment of the squared temporal gradients for *RH* (a), *TA(RH)* (b), *k* (c), *TA(k)* (d), *Vis* (e), and *TA(Vis)* (f). The straight lines are best-fits that indicate the scaling laws, and the dashed vertical lines indicate a time scale of 24 h.

3.4. Laminar Period Duration and Signal Amplitude PDFs

The PDFs of the duration of quiescent (or laminar) periods for all variables exhibit a power law decay, consistent with systems at criticality (Figure 10). In particular, Vis shows a power law scaling exponent γ close to $-3/2$. The scaling exponents for RH , k , and RH^1k_0 are lower at -1.24 , -1.25 , and -1.26 , respectively.

Equation (10) overestimates the measured spectral slope m (as in Figure 5) for all variables by differences of 0.12–0.40. When including intermittency corrections as proposed by [66], μ_s (calculated from the full series) was able to account for the difference between measured and estimated m for RH , and μ_{TA} (calculated from the TA series) was able to account for the difference for Vis . For k , neither μ_s nor μ_{TA} was able to account for the difference, showing that amplitude variations impact the relation, and the SOC model (or its corrected version for intermittency) cannot fully describe the on–off switching properties (Figure 11).

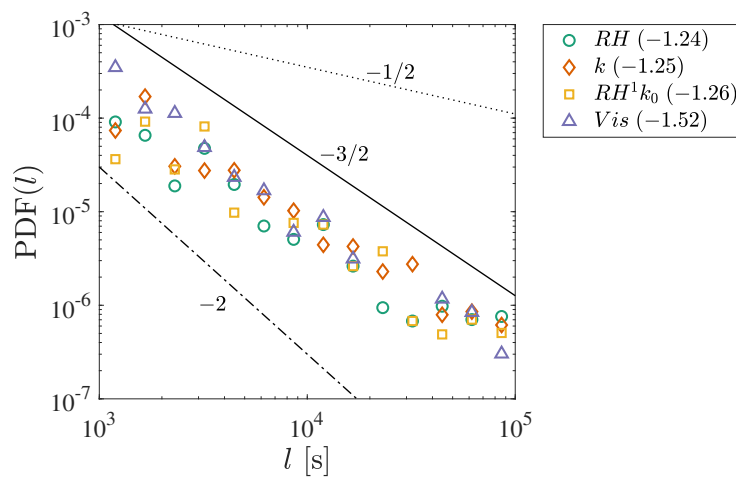


Figure 10. PDFs of the laminar period duration for RH , k , and Vis , with γ values for each variable noted in the legend. Also indicated are the scaling relations expected of a PMII process ($-1/2$), a PM2I process (-2), and a PM3I or an on–off intermittency process ($-3/2$).

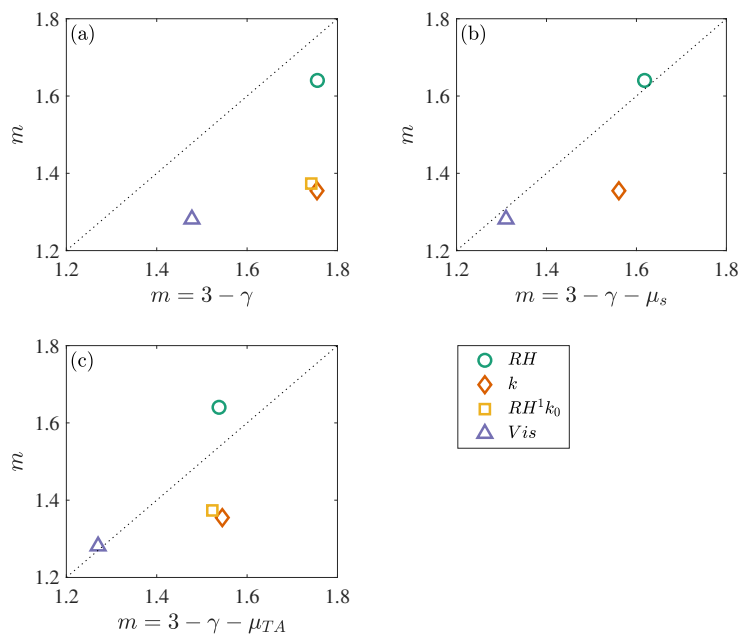


Figure 11. Measured spectral exponents of the TA spectra m (from Figure 5) against expected m of an SOC process near critical point (a) with intermittency corrections from the full series (b) and from the TA series (c). Dotted lines represent a slope of 1.

The PDFs of the signal amplitudes are shown in Figure 12 along with expected -1 and -2 slopes (see Table 1). The x -axis for $\text{PDF}(RH)$ is reversed to reflect the probability of deviating from the saturation condition. Of the three variables, only $\text{PDF}(Vis)$ exhibits a clear -2 scaling. The -2 scaling in Vis occurs over the approximate range of 300–2000 m, which envelopes the condition for fog occurrence ($Vis = 1000$ m). In $\text{PDF}(k)$, there appears to be two regimes separated at approximately $1 \text{ m}^2/\text{s}^2$ so that $\text{PDF}(k) \approx 1$ for $k < 1 \text{ m}^2/\text{s}^2$ followed by a power law decay at $k > 1 \text{ m}^2/\text{s}^2$. A scaling of -2 seems to be present only for a limited range (of approximately $k = 0.8 - 1.2 \text{ m}^2/\text{s}^2$) in the transition between the two scaling regimes. In contrast, $\text{PDF}(RH)$ has no such power law scaling.

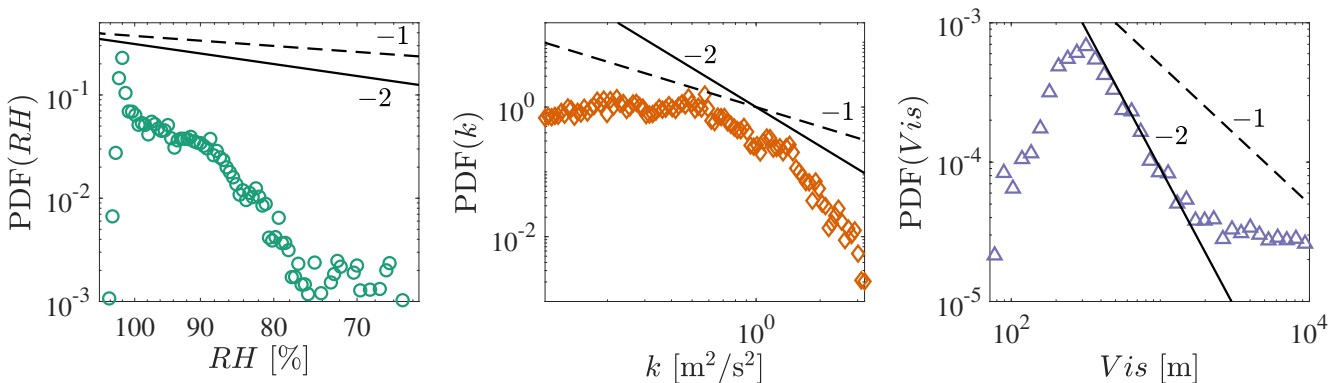


Figure 12. Signal amplitude PDFs for RH , k , and Vis . A power law scaling of -1 consistent with PM1I and on-off intermittency, and of -2 consistent with PM2I and PM3I are indicated for reference.

3.5. Block Entropy

The block entropy $H(n)$ and its growth rate with n (slope $\log \left[\frac{H(n+1)}{H(n)} \right] / \log \left[\frac{n+1}{n} \right]$) for the TA series are presented in Figure 13. For a sporadic process, the slope should converge to a constant value less than 1. All three variables appear to grow nonlinearly, and begin to reach a constant value between 0.5 and 0.6. In the context of block entropy, k appears to be the least ordered (most random), as it seems to asymptotically approach a slope of approximately 0.6. While these results suggest that RH , k , and Vis can be described as sporadically random processes, the limited n_{max} precludes conclusions on their behavior for longer time scales. It can be noted that the slope of $H(n)$ for Vis is bounded by that of RH and k at all $n > 1$, and that the RH^1k_0 series exhibits similar $H(n)$ values and growth rate to Vis .

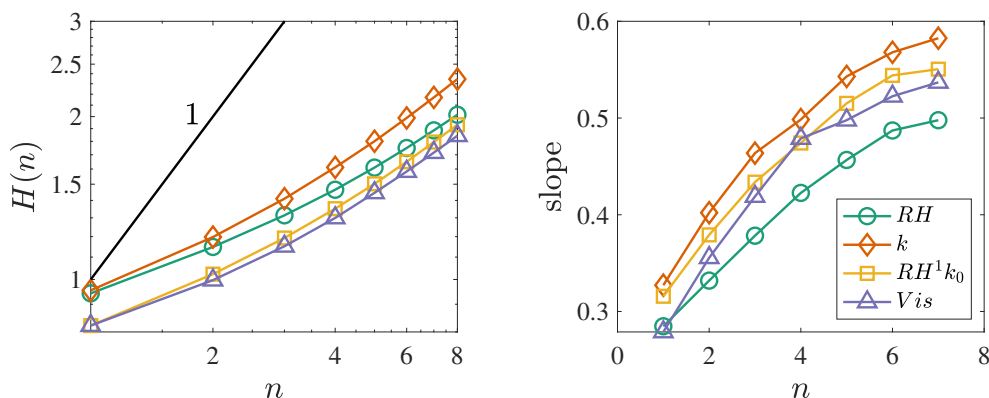


Figure 13. Block entropy $H(n)$ (left) and its slope (right) as a function of block length n . Solid line in the left panel corresponds to a slope of 1 representative of a purely random process.

4. Study Limitations

Although a longer sampling period than the current one-month dataset is best to make more affirmative conclusions, the agreement between the scaling exponents presented here and in other studies of longer duration lends credence to the results. Räsänen et al. [15] presented a longer-term analysis on fog deposition measured by a tipping bucket between June 2014 and September 2016 at a coastal site in Northern California and between October 2013 and February 2016 at an inland site in Southeastern Kenya. The TA analysis revealed that cluster exponent α , laminar period duration PDF exponent γ , and fog event size scaling exponent agree reasonably well with the exponents presented here (see Table 2), despite the differences in sampling duration. Further, the similarity of the scaling exponents shows that they may also be agnostic to the study site and measurement technique.

Table 2. Comparison of the cluster exponent α , laminar period duration PDF exponent γ , and fog event size scaling exponent from data taken on Sable Island in the current study, an inland site in Southeastern Kenya, and a coastal site in Northern California [15].

	α	γ	PDF(<i>Vis</i>)
Sable Island	0.25	1.52	~2
Inland	0.25	1.41	1.83
Coastal	0.26	1.33	1.86

Since instrument uncertainties tend to occur at high frequencies and very low frequencies, the scaling relations within the TA framework are relatively insensitive to these uncertainties in the fine scales. In fact, more extensive scaling in the TA spectra than in the full signal spectra have been observed [67]. In the current study, finite clustering persists in the fine scales for all variables considered (Figure 8) so that white noise at the very finest scales does not appear to leave a noticeable signature in the scaling exponents. That is, the fact that clear scaling laws are seen all the way across the fine scales indicates that noise is not propagating much across the time scales.

To further investigate the impact of noise to the presented conclusions, the analysis is repeated for the *Vis* series with various levels of added noise. As an estimate, the SNR for the measured *Vis* series is calculated to be 86 by treating frequencies above 1/1000 Hz as white noise (in accordance with the approximate frequency, where the spectra begins to flatten). The signal-to-noise ratio SNR of the measured signal is then progressively deteriorated by adding increasing levels of white Gaussian noise. It can be seen in Figure 14 that all scaling exponents (m , n , α , μ_s , and μ_{TA}) are approximately constant for SNR as low as 40. Similarly, the -2 scaling in PDF(*Vis*) persists for SNR as low as 40 (Figure 15). The SNR associated with the instrument is much higher than the SNR at which the scaling laws no longer hold, indicating that sensor uncertainties will not impact the conclusions presented here.

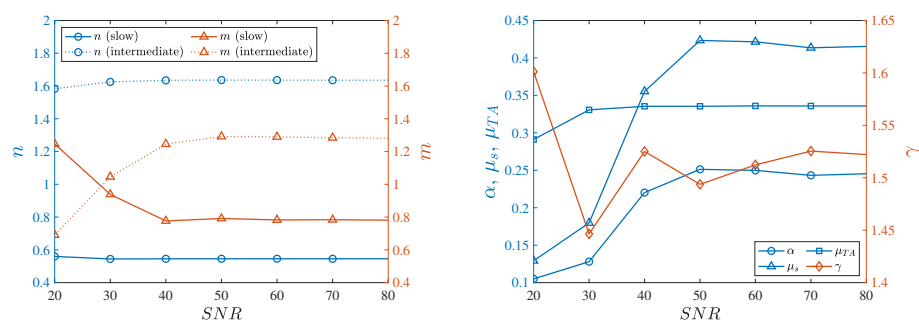


Figure 14. Spectral exponents m and n for the slow and intermediate scaling regimes as functions of SNR (left). Cluster exponent α , intermittency exponents μ_s and μ_{TA} , and scaling exponent for the laminar phase PDF γ as functions of SNR (right).

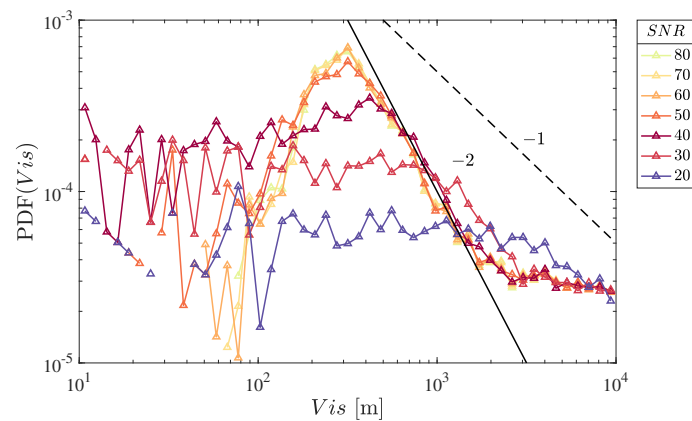


Figure 15. Signal amplitude PDFs for Vis with various SNR. Clear -2 scaling is present for SNR as low as 40.

5. Discussion and Conclusions

A preliminary analysis of the ability of RH and k , putative variables akin to the formation and breakup conditions of fog, respectively, to explain the variability in Vis through the spectra, the squared correlation coefficient, and the magnitude-squared coherence shows that RH and k play a role in fog occurrence but may not encapsulate its full dynamics. For the slow time scales (>1 d), the spectra for Vis exhibit a slower decay rate than either RH or k , which could indicate the presence of a process perhaps of meso and synoptic scales. When plotted against Vis , RH appears to be correlated to Vis ($R^2 = 0.63$), while k presents as a threshold where fog occurrence (low Vis) appears to coincide most with low k . The coherence analysis indicates that although there are certain scales where k and RH might be reasonable predictors of Vis , the stochastic behavior in Vis cannot fully be explained by RH , k , or a linear combination of the two.

Although not able to fully explain fog occurrence, RH and k bounds many stochastic features of Vis , including its spectral exponent n , clustering exponent α , and the growth of its block entropy slope. For intermediate and fine time scales (scales < 1 d), the spectral exponent of Vis ($n = 1.64$) is bounded by that of k ($n = 1.60$) and RH ($n = 1.93$). Similarly, the cluster exponent of Vis ($\alpha = 0.25$) is bounded by that of k ($\alpha = 0.26$) and RH ($\alpha = 0.24$). Lastly, the slope of $H(n)$ with n for Vis is bounded by RH and k for $n > 1$. Overall, the combined TA series RH^1k_0 reflected behavior similar to that of RH and k (i.e., in its spectral exponents, cluster exponent, intermittency exponent, and laminar phase duration distribution scaling) but did not perform significantly better than either RH or k in reproducing the stochastic features of Vis . These observations suggest that the statistics of fog are affected by those of saturation for the formation and those of turbulence for the breakup but that a linear combination of the two is too simplistic to capture the dynamics of fog.

The intermittent nature of fog was then analyzed by hypothesizing that fog is governed by one of the known intermittency models, which would inform future studies on whether and how it can be modeled. Out of the four intermittency models considered (PM1-3I and on-off), the Vis series under study presents features of PM3I in its power spectrum scaling (which approaches $-1/2$ as $f \rightarrow 0$), signal amplitude distribution scaling (a power law decay with an exponent of -2 over almost a decade), and laminar phase duration distribution scaling (a power law decay with an exponent of $-3/2$ for $l < 24$ h). These features were not observed in the RH or k series. More generally, PM3I can be viewed as an example of sporadic randomness, which describes systems between purely random and purely deterministic behaviors. Preliminary analysis of the block entropy growth based on the TA series indicates sub-linear behaviors consistent with sporadic randomness. Although limited by the sample length, the slope of $H(n)$ appears to reach a constant as n increases for all three variables. Qualitatively, PM3I entails a slow accumulation followed by a random re-injection or relaxation. The intermittency in fog is driven by the

dynamics of the atmospheric boundary layer, where the atmospheric water vapor slowly accumulates (the rising limb of the characteristic PM3I processes) under proper moisture and heating conditions (encoded in RH) and is then 're-injected' whenever turbulence levels are high (and presumed to be stochastic). Identifying the physical origin of this intermittency remains an open question, as many variables (e.g., meteorological variables, aerosols, and wave breaking, some of which are interrelated) occurring at various time scales affect the life cycle of fog.

While intermittent behavior emerges as the system heads to chaotic behavior, SOC describes the phase transition between an ordered and a disordered state. Here, the ordered states are the no-fog phases, while the disordered states are fog intensities (represented here by the Vis time series). In finite systems, the critical point between second-order phase transitions is smoothed out over a small interval, so the coexistence between some features of no-fog phases (high k) and the presence of fog could then indicate that the system is at criticality. The integral time scales associated with each variable are calculated and presented in Table 3. For the full series, the integral time scale for k (10.3 h) appears to be slightly longer than that of RH (7.6 h) and Vis (8.0 h). For the binary TA series, the integral time scales for all three variables are commensurate, ranging from 6.9 to 7.6 h such that there seems to be a single relaxation time scale that governs the token formation and breakup process of fog, at least in their clustering tendencies.

Table 3. Integral time scales of the full and TA series in hours.

	RH	k	Vis
Full	7.6	10.3	8.0
TA	7.6	7.1	6.9

Thus, a simplistic physical model that lends itself to such phase transitions and criticality emerges where the activation mechanism for fog arises from thermodynamic interactions while the deactivation mechanism arises from turbulence. For fog events to occur, an air mass must become saturated near the earth's surface, and a sufficient amount of fog condensation nuclei (e.g., sea salts in marine fog) must be present to generate small airborne water droplets (1–30 μm in diameter) that remain suspended. Turbulence (and possibly background winds, which are related to k) then serves as the destructive or deactivating mechanism that dissipates fog. That is, fog is 'deactivated' if the turbulence becomes strong enough, and 'activated' if turbulence is weak enough, provided that air is saturated and condensation nuclei are present. The ensuing dynamics encapsulating these arguments may be expressed by [57]

$$\frac{dA}{dt} = \frac{A}{\tau_o} [\alpha_o(1 - A) - \beta_o], \quad (12)$$

where $A = 0$ is a no-fog state, $A = 1$ is a full fog (or $Vis = 0$), τ_o reflects the fog formation time, α_o is related to the thermodynamic state for fog formation (e.g., $\alpha_o = 0$ for low RH and unity for $RH = 1$), and β_o is related to k ($\beta_o = 0$ for low k and $\beta_o = 1$ for high k). This system exhibits two equilibrium states: $A = 0$ (no fog) and $A = 1 - \beta_o/\alpha_o$ (fog). The activation phase occurs through α_o (or RH) and the deactivation phase is associated with a correlated random β_o (linked to k). In the absence of turbulence ($\beta_o = 0$) but for finite α_o , A will gradually increase until steady-state $dA/dt = 0$ conditions prevail ($A = 1$). These conditions are sporadically 'broken' by either a small α_o (thermodynamic considerations no longer support fog such as advection or entrainment of dry or warm air) or a large β_o (high level of turbulence breaking up the fog). Fog formation necessitates $\beta_o/\alpha_o < 1$. Other mechanisms that dissipate fog beyond turbulence not considered here but worth investigating in future studies include radiation, lack of water vapor sustained in the atmosphere, particle coalescence, or loss of particles near the ground that could serve as condensation nuclei (and all impact α_o to a leading order).

The aim of this paper was to investigate whether SOC describes fog occurrence is based on its universal stochastic patterns in the form of power laws and scale invariance (in time or space or both) in complex systems. The current *Vis* series exhibits power laws in its amplitude distribution, spectra, clustering, and laminar period duration distribution, permitting an evaluation of the relation between the measured exponent of the TA spectra m and the exponent of the laminar period duration scaling γ expected for an SOC system at criticality ($m = 3 - \gamma$). This SOC relation was observed in *Vis* and in *RH* only after intermittency corrections ($m = 3 - \gamma - \mu$). In *RH*, this was achieved with the intermittency coefficient calculated from the full series ($\mu = \mu_s$), while incorporating μ_{TA} calculated from the TA series overestimates the measured m . In *Vis*, intermittency correction from the TA series ($\mu = \mu_{TA}$) was needed to achieve the SOC relation. These observations further suggest that fog events, or the underlying formation mechanisms associated with *RH*, could be SOC processes, albeit the education of information needing intermittency corrections.

In celebration of Dr. Herring's career and life work in geophysical fluid dynamics [78,79], stochastic approaches to turbulence [80,81], and the intermittency of high Reynolds number turbulence in particular, this paper presents a statistical analysis of fog and two of its underlying atmospheric variables—turbulent kinetic energy and relative humidity—in relation to its intermittency and self-organized critical behavior. Overall, this study identified the qualitative dynamical features of fog (through its visibility time series) and of the two variables that govern its formation and dissipation. Although not diagnostic, phenomenological properties of PM3I were observed in the *Vis* series, which may be more generally described by a sporadically random process. The results presented also conform with elements of self-organized criticality in its on-off and off-on switching properties. These features and similarities to known dynamical models in literature can be sought in future modeling efforts to reproduce the stochastic properties of fog in a broad range of time scales or as validation. Since many atmospheric variables and physical mechanisms affect the formation, duration, and dissolution of fog, the physical origin and exact analogy to SOC or PM3I, especially under different fog-formation conditions, remain an open question suggested for future inquiries.

Author Contributions: Conceptualization, K.Y.H. and G.G.K.; Data curation, K.Y.H., T.J.H. and J.R.-P.; Formal analysis, K.Y.H.; Funding acquisition, Q.W. and H.J.S.F.; Investigation, K.Y.H., T.J.H., J.R.-P. and Q.W.; Methodology, G.G.K.; Project administration, Q.W. and H.J.S.F.; Software, G.G.K.; Visualization, K.Y.H.; Writing—original draft, K.Y.H.; Writing—review and editing, G.G.K., T.J.H., J.R.-P., Q.W. and H.J.S.F. All authors have read and agreed to the published version of the manuscript.

Funding: K.Y.H., T.J.H., J.R.-P., Q.W. and H.J.S.F. were funded by the Grant N00014-21-1-2296 (Fatima Multidisciplinary University Research Initiative) of the Office of Naval Research, administered by the Marine Meteorology and Space Program. G.G.K. acknowledges partial support from the U.S. National Science Foundation (NSF-AGS-2028633) and the Department of Energy (DE-SC0022072).

Institutional Review Board Statement: Not applicable.

Informed Consent Statement: Not applicable.

Data Availability Statement: Data are available upon request.

Acknowledgments: The authors would like to thank the field research team of Sable Island, Parks Canada—Marvin Willis and Paul LeBlanc—for their invaluable assistance with project operations.

Conflicts of Interest: The authors declare no conflict of interest.

References

1. Myers, J.N. Fog. *Sci. Am.* **1968**, *219*, 74–83. [[CrossRef](#)]
2. Shrestha, S.; Moore, G.A.; Peel, M.C. Trends in winter fog events in the Terai region of Nepal. *Agric. For. Meteorol.* **2018**, *259*, 118–130. [[CrossRef](#)]
3. Baldocchi, D.; Waller, E. Winter fog is decreasing in the fruit growing region of the Central Valley of California. *Geophys. Res. Lett.* **2014**, *41*, 3251–3256. [[CrossRef](#)]

4. Klemm, O.; Schemenauer, R.S.; Lummerich, A.; Cereceda, P.; Marzol, V.; Corell, D.; Van Heerden, J.; Reinhard, D.; Gherezghiher, T.; Olivier, J.; et al. Fog as a fresh-water resource: Overview and perspectives. *Ambio* **2012**, *41*, 221–234. [[CrossRef](#)]
5. Montecinos, S.; Carvajal, D.; Cereceda, P.; Concha, M. Collection efficiency of fog events. *Atmos. Res.* **2018**, *209*, 163–169. [[CrossRef](#)]
6. Salcedo-Sanz, S.; Piles, M.; Cuadra, L.; Casanova-Mateo, C.; Caamaño, A.; Cerro-Prada, E.; Camps-Valls, G. Long-term persistence, invariant time scales and on-off intermittency of fog events. *Atmos. Res.* **2021**, *252*, 105456. [[CrossRef](#)]
7. Foufoula-Georgiou, E.; Krajewski, W. Recent advances in rainfall modeling, estimation, and forecasting. *Rev. Geophys.* **1995**, *33*, 1125–1137. [[CrossRef](#)]
8. Georgakakos, K.P.; Kavvas, M.L. Precipitation analysis, modeling, and prediction in hydrology. *Rev. Geophys.* **1987**, *25*, 163–178. [[CrossRef](#)]
9. Gupta, V.K.; Waymire, E. Multiscaling properties of spatial rainfall and river flow distributions. *J. Geophys. Res. Atmos.* **1990**, *95*, 1999–2009. [[CrossRef](#)]
10. Menabde, M.; Harris, D.; Seed, A.; Austin, G.; Stow, D. Multiscaling properties of rainfall and bounded random cascades. *Water Resour. Res.* **1997**, *33*, 2823–2830. [[CrossRef](#)]
11. Olsson, J.; Burlando, P. Reproduction of temporal scaling by a rectangular pulses rainfall model. *Hydrol. Process.* **2002**, *16*, 611–630. [[CrossRef](#)]
12. Rigby, J.; Porporato, A. Precipitation, dynamical intermittency, and sporadic randomness. *Adv. Water Resour.* **2010**, *33*, 923–932. [[CrossRef](#)]
13. Peters, O.; Neelin, J.D. Critical phenomena in atmospheric precipitation. *Nat. Phys.* **2006**, *2*, 393–396. [[CrossRef](#)]
14. Bak, P.; Chen, K. Self-organized criticality. *Sci. Am.* **1991**, *264*, 46–53. [[CrossRef](#)]
15. Räsänen, M.; Chung, M.; Katurji, M.; Pellikka, P.; Rinne, J.; Katul, G. Similarity in fog and rainfall intermittency. *Geophys. Res. Lett.* **2018**, *45*, 10–691. [[CrossRef](#)]
16. Bergé, P.; Pomeau, Y.; Vidal, C. *Order Within Chaos*; Wiley: Hoboken, NJ, USA, 1987.
17. Lakshmanan, M.; Rajaseekar, S. *Nonlinear Dynamics: Integrability, Chaos and Patterns*; Springer Science & Business Media: Berlin/Heidelberg, Germany, 2012.
18. Pomeau, Y.; Manneville, P. Intermittent transition to turbulence in dissipative dynamical systems. In *Universality in Chaos*; Routledge: Abingdon-on-Thames, UK, 2017; pp. 327–335.
19. Hirsch, J.; Huberman, B.; Scalapino, D. Theory of intermittency. *Phys. Rev. A* **1982**, *25*, 519. [[CrossRef](#)]
20. Scholz, H.; Yamada, T.; Brand, H.; Graham, R. Intermittency and chaos in a laser system with modulated inversion. *Phys. Lett. A* **1981**, *82*, 321–323. [[CrossRef](#)]
21. Meunier, C.; Bussac, M.N.; Laval, G. Intermittency at the onset of stochasticity in nonlinear resonant coupling processes. *Phys. D Nonlinear Phenom.* **1982**, *4*, 236–243. [[CrossRef](#)]
22. Pomeau, Y.; Roux, J.; Rossi, A.; Bachelart, S.; Vidal, C. Intermittent behaviour in the Belousov-Zhabotinsky reaction. *J. De Phys. Lettres* **1981**, *42*, 271–273. [[CrossRef](#)]
23. Bergé, P.; Dubois, M.; Manneville, P.; Pomeau, Y. Intermittency in Rayleigh-Bénard convection. *J. De Phys. Lettres* **1980**, *41*, 341–345. [[CrossRef](#)]
24. Maurer, J.; Libchaber, A. Effect of the Prandtl number on the onset of turbulence in liquid 4He. *J. De Phys. Lettres* **1980**, *41*, 515–518. [[CrossRef](#)]
25. Jeffries, C.; Perez, J. Observation of a Pomeau-Manneville intermittent route to chaos in a nonlinear oscillator. *Phys. Rev. A* **1982**, *26*, 2117. [[CrossRef](#)]
26. Richetti, P.; Argoul, F.; Arneodo, A. Type-II intermittency in a periodically driven nonlinear oscillator. *Phys. Rev. A* **1986**, *34*, 726. [[CrossRef](#)] [[PubMed](#)]
27. Huang, J.Y.; Kim, J.J. Type-II intermittency in a coupled nonlinear oscillator: Experimental observation. *Phys. Rev. A* **1987**, *36*, 1495. [[CrossRef](#)] [[PubMed](#)]
28. Ringuet, E.; Rozé, C.; Gouesbet, G. Experimental observation of type-II intermittency in a hydrodynamic system. *Phys. Rev. E* **1993**, *47*, 1405. [[CrossRef](#)]
29. Velazquez, J.P.; Khosravani, H.; Lozano, A.; Bardakjian, B.L.; Carlen, P.L.; Wennberg, R. Type III intermittency in human partial epilepsy. *Eur. J. Neurosci.* **1999**, *11*, 2571–2576. [[CrossRef](#)]
30. Griffith, T.; Parthimos, D.; Crombie, J.; Edwards, D.H. Critical scaling and type-III intermittent chaos in isolated rabbit resistance arteries. *Phys. Rev. E* **1997**, *56*, R6287. [[CrossRef](#)]
31. Richter, R.; Peinke, J.; Clauss, W.; Rau, U.; Parisi, J. Evidence of type-III intermittency in the electric breakdown of p-type germanium. *EPL (Europhys. Lett.)* **1991**, *14*, 1. [[CrossRef](#)]
32. Kahn, A.; Mar, D.; Westervelt, R. Spatial measurements near the instability threshold in ultrapure Ge. *Phys. Rev. B* **1992**, *45*, 8342. [[CrossRef](#)]
33. Ono, Y.; Fukushima, K.; Yazaki, T. Critical behavior for the onset of type-III intermittency observed in an electronic circuit. *Phys. Rev. E* **1995**, *52*, 4520. [[CrossRef](#)]
34. Kim, C.M.; Yim, G.S.; Ryu, J.W.; Park, Y.J. Characteristic relations of type-III intermittency in an electronic circuit. *Phys. Rev. Lett.* **1998**, *80*, 5317. [[CrossRef](#)]

35. Dubois, M.; Rubio, M.; Berge, P. Experimental evidence of intermittencies associated with a subharmonic bifurcation. *Phys. Rev. Lett.* **1983**, *51*, 1446. [[CrossRef](#)]
36. Platt, N.; Spiegel, E.; Tresser, C. On-off intermittency: A mechanism for bursting. *Phys. Rev. Lett.* **1993**, *70*, 279. [[CrossRef](#)] [[PubMed](#)]
37. Pikovsky, A. On the interaction of strange attractors. *Z. Für Phys. B Condens. Matter* **1984**, *55*, 149–154. [[CrossRef](#)]
38. Fujisaka, H.; Yamada, T. A new intermittency in coupled dynamical systems. *Prog. Theor. Phys.* **1985**, *74*, 918–921. [[CrossRef](#)]
39. Heagy, J.; Platt, N.; Hammel, S. Characterization of on-off intermittency. *Phys. Rev. E* **1994**, *49*, 1140. [[CrossRef](#)]
40. Yu, Y.H.; Kwak, K.; Lim, T.K. On-off intermittency in an experimental synchronization process. *Phys. Lett. A* **1995**, *198*, 34–38. [[CrossRef](#)]
41. Hammer, P.W.; Platt, N.; Hammel, S.M.; Heagy, J.F.; Lee, B.D. Experimental observation of on-off intermittency. *Phys. Rev. Lett.* **1994**, *73*, 1095. [[CrossRef](#)]
42. Rödelberger, F.; Čenys, A.; Benner, H. On-off intermittency in spin-wave instabilities. *Phys. Rev. Lett.* **1995**, *75*, 2594. [[CrossRef](#)]
43. Feng, D.; Yu, C.; Xie, J.; Ding, W. On-off intermittencies in gas discharge plasma. *Phys. Rev. E* **1998**, *58*, 3678. [[CrossRef](#)]
44. John, T.; Stannarius, R.; Behn, U. On-off intermittency in stochastically driven electrohydrodynamic convection in nematics. *Phys. Rev. Lett.* **1999**, *83*, 749. [[CrossRef](#)]
45. Bauer, M.; Habip, S.; He, D.R.; Martienssen, W. New type of intermittency in discontinuous maps. *Phys. Rev. Lett.* **1992**, *68*, 1625. [[CrossRef](#)] [[PubMed](#)]
46. He, D.R.; Wang, D.K.; Shi, K.J.; Yang, C.h.; Chao, L.y.; Zhang, J.Y. Critical behavior of dynamical systems described by the inverse circle map. *Phys. Lett. A* **1989**, *136*, 363–368. [[CrossRef](#)]
47. Price, T.; Mullin, T. An experimental observation of a new type of intermittency. *Phys. D Nonlinear Phenom.* **1991**, *48*, 29–52. [[CrossRef](#)]
48. San-Martin, J.; Antoranz, J. Type-II intermittency with a double reinjection channel: Multintermittency. *Phys. Lett. A* **1996**, *219*, 69–73. [[CrossRef](#)]
49. Grebogi, C.; Ott, E.; Yorke, J.A. Crises, sudden changes in chaotic attractors, and transient chaos. *Phys. D Nonlinear Phenom.* **1983**, *7*, 181–200. [[CrossRef](#)]
50. Schuster, H.G.; Just, W. *Deterministic Chaos: An Introduction*; John Wiley & Sons: Hoboken, NJ, USA, 2006.
51. Procaccia, I.; Schuster, H. Functional renormalization-group theory of universal $1/f$ noise in dynamical systems. *Phys. Rev. A* **1983**, *28*, 1210. [[CrossRef](#)]
52. Venkataramani, S.C.; Antonsen, T.M., Jr.; Ott, E.; Sommerer, J.C. On-off intermittency: Power spectrum and fractal properties of time series. *Phys. D Nonlinear Phenom.* **1996**, *96*, 66–99. [[CrossRef](#)]
53. Toniolo, C.; Provenzale, A.; Spiegel, E.A. Signature of on-off intermittency in measured signals. *Phys. Rev. E* **2002**, *66*, 066209. [[CrossRef](#)]
54. Gaspard, P.; Wang, X.J. Sporadicity: Between periodic and chaotic dynamical behaviors. *Proc. Natl. Acad. Sci. USA* **1988**, *85*, 4591–4595. [[CrossRef](#)]
55. Legenstein, R.; Maass, W. Edge of chaos and prediction of computational performance for neural circuit models. *Neural Netw.* **2007**, *20*, 323–334. [[CrossRef](#)] [[PubMed](#)]
56. Grieger, B. Quaternary climatic fluctuations as a consequence of self-organized criticality. *Phys. A Stat. Mech. Its Appl.* **1992**, *191*, 51–56. [[CrossRef](#)]
57. Hesse, J.; Gross, T. Self-organized criticality as a fundamental property of neural systems. *Front. Syst. Neurosci.* **2014**, *8*, 166. [[CrossRef](#)] [[PubMed](#)]
58. Roberts, D.C.; Turcotte, D.L. Fractality and self-organized criticality of wars. *Fractals* **1998**, *6*, 351–357. [[CrossRef](#)]
59. Turcotte, D.L. Self-organized criticality. *Rep. Prog. Phys.* **1999**, *62*, 1377. [[CrossRef](#)]
60. Jensen, H.J. *Self-Organized Criticality: Emergent Complex Behavior in Physical and Biological Systems*; Cambridge University Press: Cambridge, UK, 1998; Volume 10.
61. Pruessner, G. *Self-Organised Criticality: Theory, Models and Characterisation*; Cambridge University Press: Cambridge, UK, 2012.
62. Dorman, C.E.; Mejia, J.; Koračin, D.; McEvoy, D. Worldwide marine fog occurrence and climatology. In *Marine Fog: Challenges and Advancements in Observations, Modeling, and Forecasting*; Springer: Berlin/Heidelberg, Germany, 2017; pp. 7–152.
63. Horst, T.; Oncley, S. Corrections to inertial-range power spectra measured by CSAT3 and Solent sonic anemometers, 1. Path-averaging errors. *Bound. Layer Meteorol.* **2006**, *119*, 375–395. [[CrossRef](#)]
64. Horst, T.; Semmer, S.; Maclean, G. Correction of a non-orthogonal, three-component sonic anemometer for flow distortion by transducer shadowing. *Bound. Layer Meteorol.* **2015**, *155*, 371–395. [[CrossRef](#)]
65. Gulpepe, I.; Milbrandt, J.A.; Zhou, B. Marine fog: A review on microphysics and visibility prediction. In *Marine Fog: Challenges and Advancements in Observations, Modeling, and Forecasting*; Springer: Berlin/Heidelberg, Germany, 2017; pp. 345–394.
66. Bershadskii, A.; Niemela, J.; Praskovsky, A.; Sreenivasan, K. "Clusterization" and intermittency of temperature fluctuations in turbulent convection. *Phys. Rev. E* **2004**, *69*, 056314. [[CrossRef](#)]
67. Sreenivasan, K.; Bershadskii, A. Clustering properties in turbulent signals. *J. Stat. Phys.* **2006**, *125*, 1141–1153. [[CrossRef](#)]
68. Poggi, D.; Katul, G. Flume experiments on intermittency and zero-crossing properties of canopy turbulence. *Phys. Fluids* **2009**, *21*, 065103. [[CrossRef](#)]

69. Cava, D.; Katul, G. The effects of thermal stratification on clustering properties of canopy turbulence. *Bound. Layer Meteorol.* **2009**, *130*, 307–325. [[CrossRef](#)]
70. Cava, D.; Katul, G.G.; Molini, A.; Elefante, C. The role of surface characteristics on intermittency and zero-crossing properties of atmospheric turbulence. *J. Geophys. Res. Atmos.* **2012**, *117*, 1–17. [[CrossRef](#)]
71. Cava, D.; Mortarini, L.; Giostra, U.; Acevedo, O.; Katul, G. Submeso motions and intermittent turbulence across a nocturnal low-level jet: A self-organized criticality analogy. *Bound. Layer Meteorol.* **2019**, *172*, 17–43. [[CrossRef](#)]
72. Heisel, M.; Katul, G.G.; Chamecki, M.; Guala, M. Velocity asymmetry and turbulent transport closure in smooth-and rough-wall boundary layers. *Phys. Rev. Fluids* **2020**, *5*, 104605. [[CrossRef](#)]
73. Chowdhuri, S.; Kalmár-Nagy, T.; Banerjee, T. Persistence analysis of velocity and temperature fluctuations in convective surface layer turbulence. *Phys. Fluids* **2020**, *32*, 076601. [[CrossRef](#)]
74. Huang, K.Y.; Katul, G.G.; Hultmark, M. Velocity and temperature dissimilarity in the surface layer uncovered by the telegraph approximation. *Bound. Layer Meteorol.* **2021**, *180*, 385–405. [[CrossRef](#)]
75. Molini, A.; Katul, G.G.; Porporato, A. Revisiting rainfall clustering and intermittency across different climatic regimes. *Water Resour. Res.* **2009**, *45*. [[CrossRef](#)]
76. Shannon, C.E. A mathematical theory of communication. *Bell Syst. Tech. J.* **1948**, *27*, 379–423. [[CrossRef](#)]
77. Jensen, H.J.; Christensen, K.; Fogedby, H.C. $1/f$ noise, distribution of lifetimes, and a pile of sand. *Phys. Rev. B* **1989**, *40*, 7425. [[CrossRef](#)]
78. Herring, J.R.; Cermak, J.E.; Neu, W.L.; Richardson, E.V.; Diplas, P.; Rand, R.H.; Yates, G.T.; Spedding, G.R.; de Laurier, J.D.; Houtt, D.P.; et al. Fluid Dynamics in Nature. *Handb. Fluid Dyn. Fluid Mach. Appl. Fluid Dyn.* **1996**, *3*, 1847–1989.
79. Herring, J. A Brief History of the Geophysical Turbulence Program at NCAR. In *Proceedings of the IUTAM Symposium on Developments in Geophysical Turbulence*; Springer: Berlin/Heidelberg, Germany, 2000; pp. 1–4.
80. Herring, J.R. Chapter 4: An Introduction and Overview of Various Theoretical Approaches to Turbulence. In *Applied Mathematical Sciences*; Springer: Berlin/Heidelberg, Germany, 1985; Volume 58, p. 73.
81. Herring, J. The role of statistical models in turbulence. *Stoch. Model. Geosystems* **2012**, *85*, 129.

Disclaimer/Publisher’s Note: The statements, opinions and data contained in all publications are solely those of the individual author(s) and contributor(s) and not of MDPI and/or the editor(s). MDPI and/or the editor(s) disclaim responsibility for any injury to people or property resulting from any ideas, methods, instructions or products referred to in the content.